Supplementary Information

Magnetic Study of a Layered Lanthanide Hydroxide Family: $Ln_8(OH)_{20}Cl_4 \bullet nH_2O$ (Ln = Tb, Ho, Er)

Joana T. Coutinho,[a,b] Claudia C. L. Pereira,[c] Joaquim Marçalo,[a,d] José J. Baldoví,[e*] Manuel Almeida,[a] Bernardo Monteiro,[a,d*] Laura C. J. Pereira[a*]

[a]Centro de Ciências e Tecnologias Nucleares (C2TN), Instituto Superior Técnico, Universidade de Lisboa, Campus Tecnológico e Nuclear, Estrada Nacional 10, 2695-066 Bobadela, Portugal.
[b]Instituto de Ciencia Molecular (ICMol), Universidad de Valencia, Catedrático José Beltrán 2, 46980 Paterna, Valencia, Spain.
[c]LAQV-REQUIMTE, Dep. de Química, Universidade Nova de Lisboa,2829-516, Monte de Caparica, Portugal
[d]Centro de Química Estrutural (CQE), Instituto Superior Técnico, Universidade de Lisboa, Campus Tecnológico e Nuclear, Estrada Nacional 10, 2695-066 Bobadela, Portugal
[e]Max Planck Institute for the Structure and Dynamics of Matter, Luruper Chaussee 149, D-22761 Hamburg, Germany.

Contents:

1) Powder XRD patterns

2) Thermogravimetry

3) Experimental magnetic data

    a) DC measurements

    b) AC measurements

4) Radial effective charge (REC) model

1) Powder XRD patterns
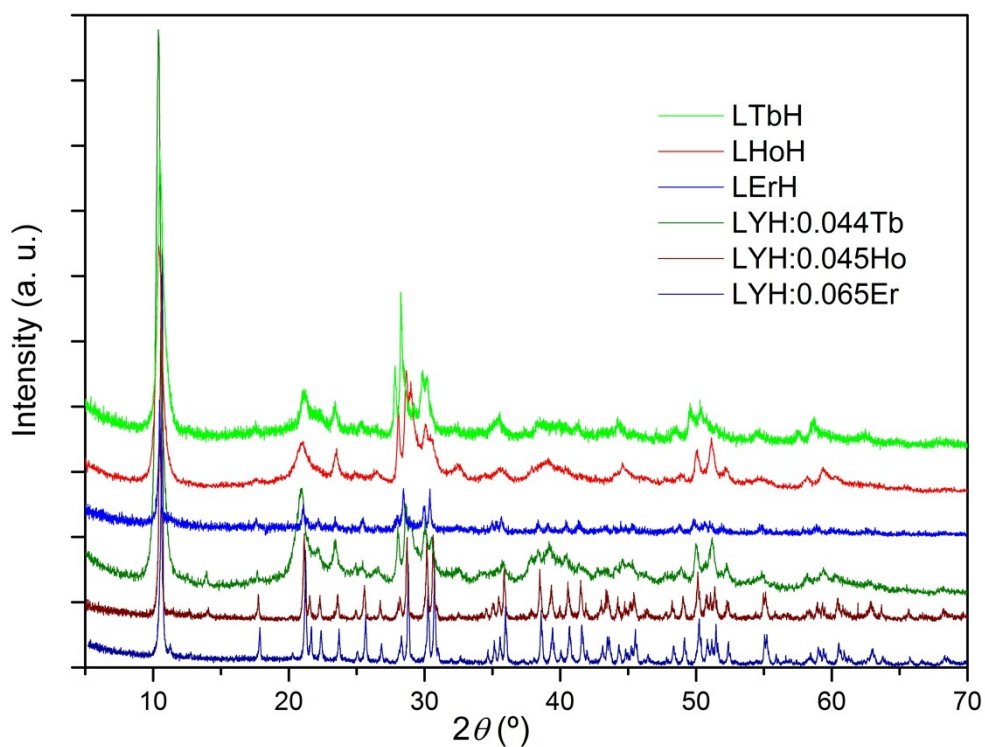

Figure S1. XRPD patterns of LTbH. LHoH, LErH, LYH:0.044Tb, LYH:0.045Ho and LYH:0.065Er (Cu K$_\alpha$ radiation).
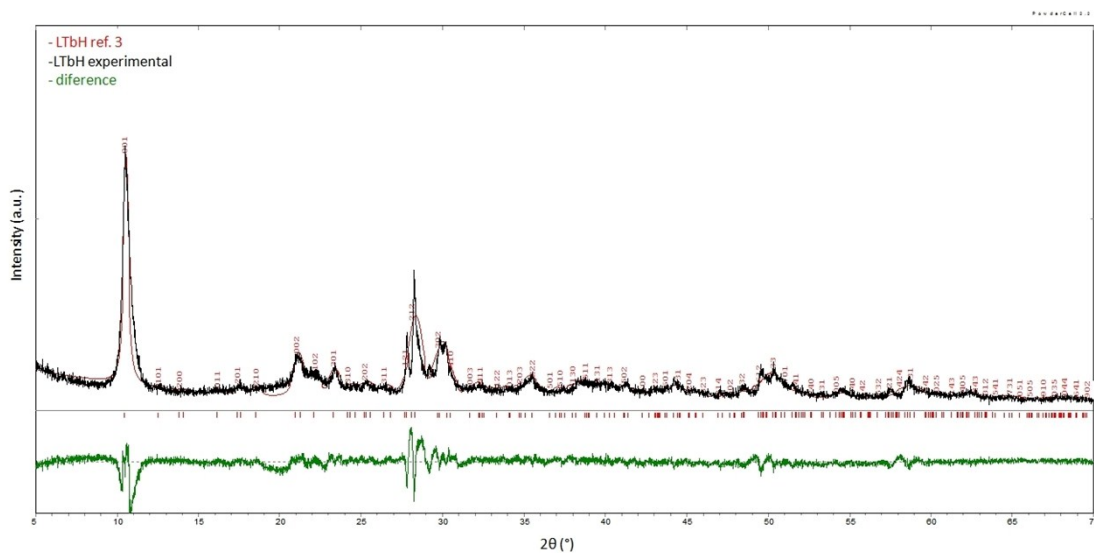

Figure S2. Le Bail whole pattern fitting of LTbH (**1**) with LTbH crystallographic data from ref. 1 using Powder Cell.
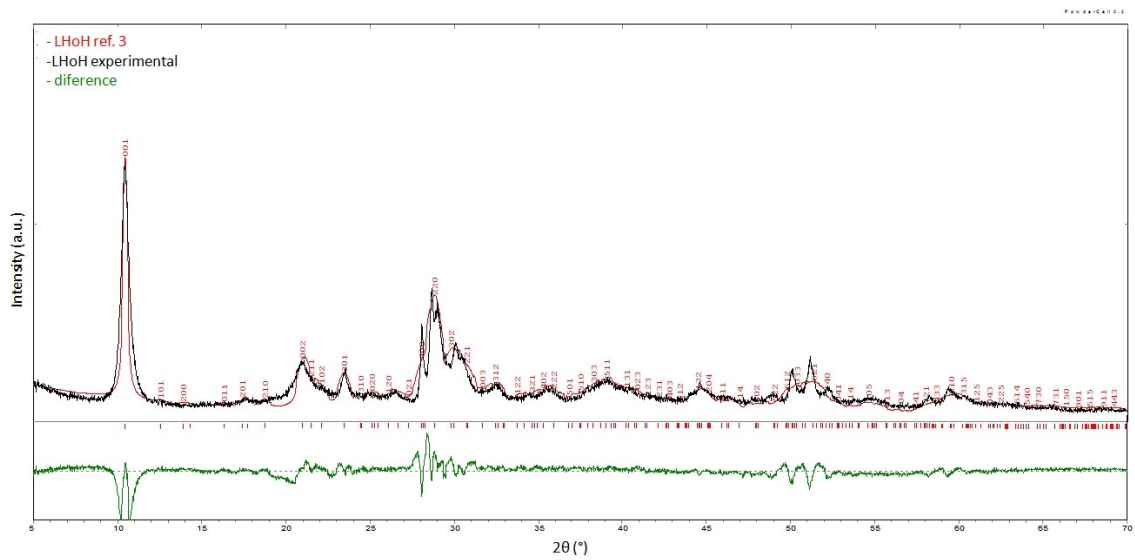
Figure S3. Le Bail whole pattern fitting of LHoH (**2**) with LHoH crystallographic data from ref. 1 using Powder Cell.
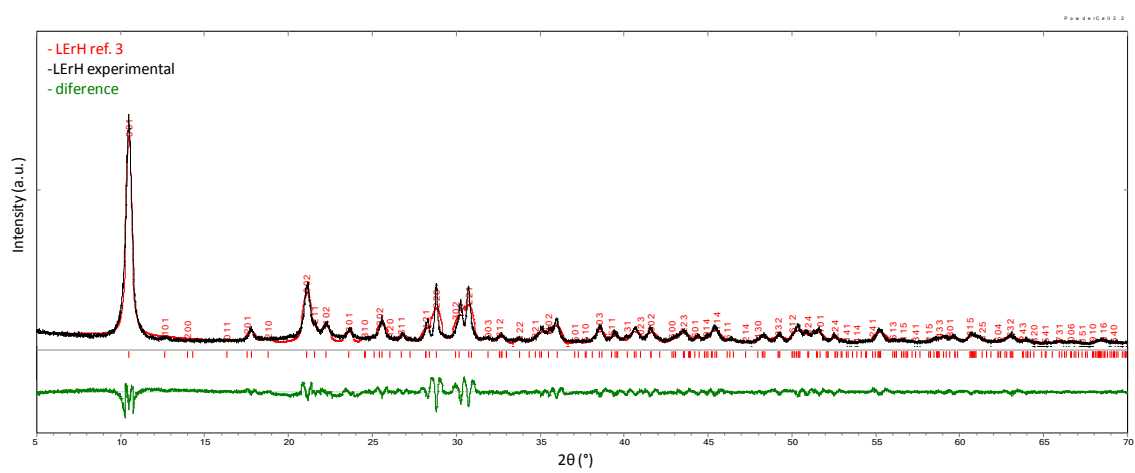

Figure S4. Le Bail whole pattern fitting of LErH (**3**) with LErH crystallographic data from ref. 1 using Powder Cell.
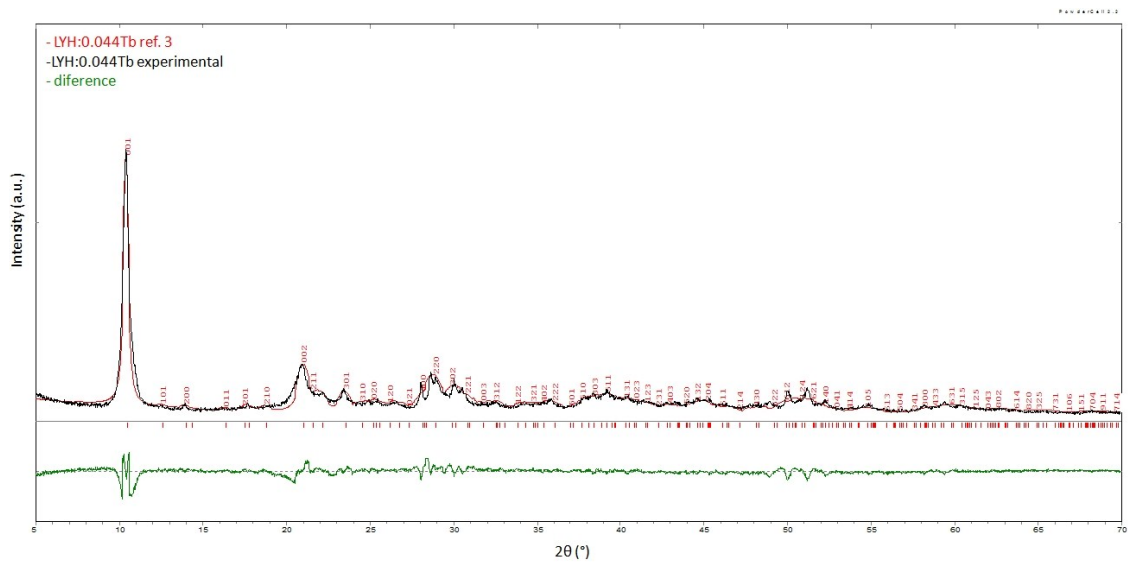
Figure S5. Le Bail whole pattern fitting of LYH:0.044Tb (**1'**) with LYH crystallographic data from ref. 1 using Powder Cell.
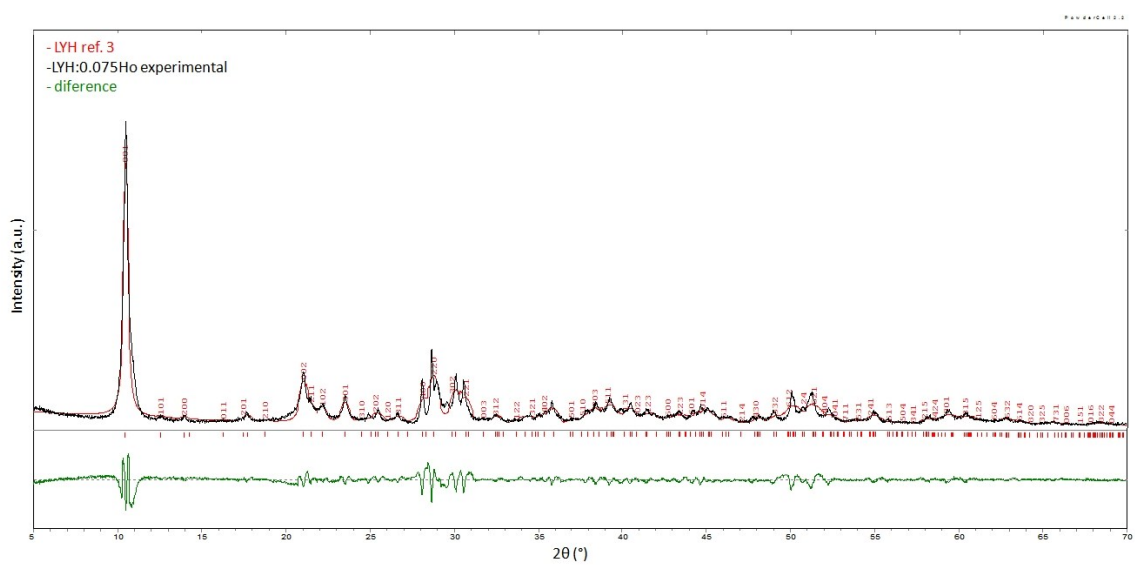

Figure S6. Le Bail whole pattern fitting of LYH:0.045Ho (**2'**) with LYH crystallographic data from ref. 1 using Powder Cell.
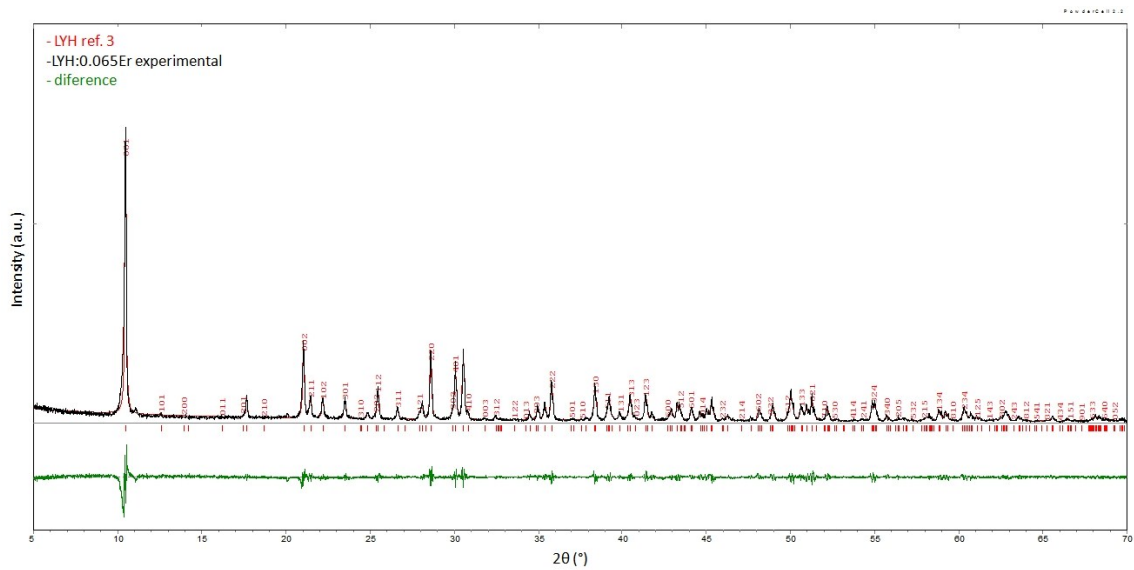
Figure S7. Le Bail whole pattern fitting of LYH:0.065Er (**3'**) with LYH crystallographic data from ref. 1 using Powder Cell.

2) Thermogravimetry

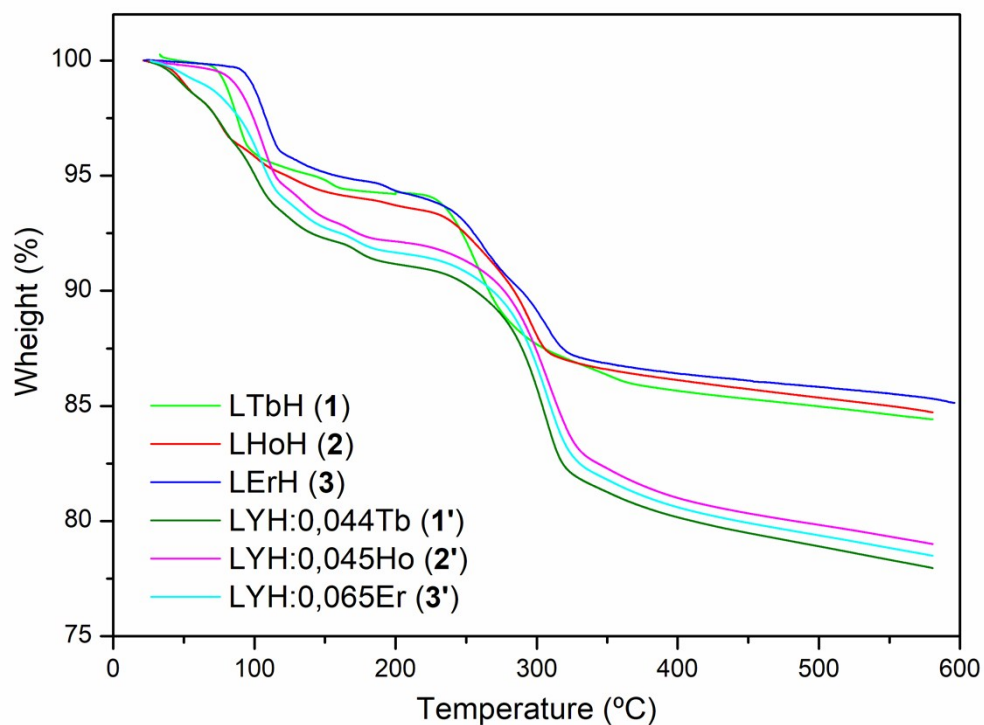**Figure S8.** TGA thermograms results of the undiluted LTbH (**1**, green), LHoH (**2**, red), LErH (**3**, blue) and diluted LYH:0.044Tb (**1'**, olive), LYH:0.045Ho (**2'**, pink) and LYH:0.065Er (**3'**, light blue) compounds.

2) Experimental magnetic data

a) DC measurements
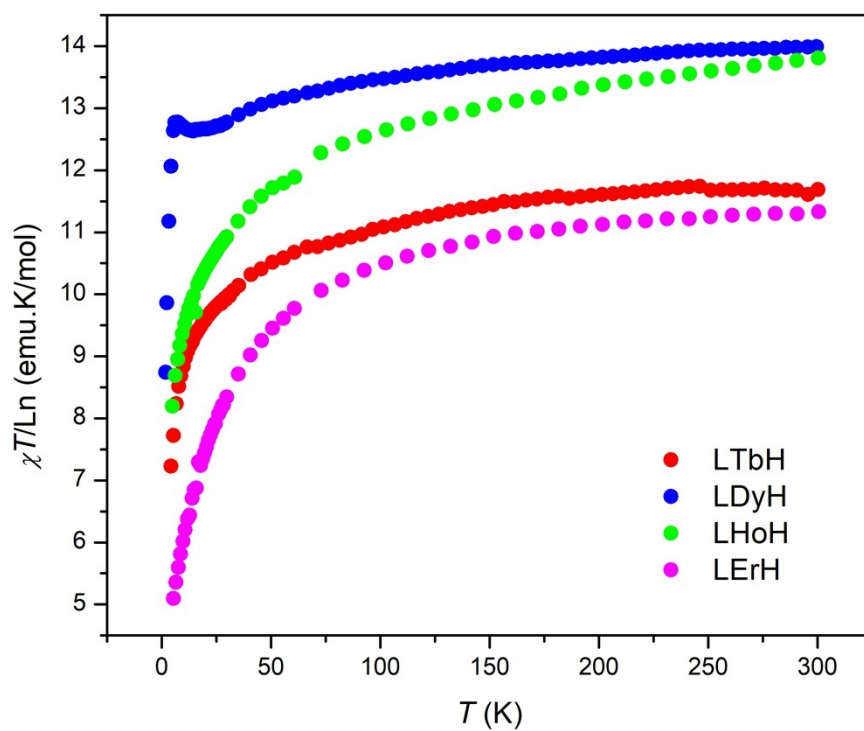
Figure S9: Magnetic susceptibility of the undiluted Ln compounds, in the temperature range 5-300 K, under a magnetic field of 100 G.

Figure S10. Field dependence of the magnetization at several temperatures for (a) LHoH (**2**) and (b) LYH:0.045Ho (**2'**).
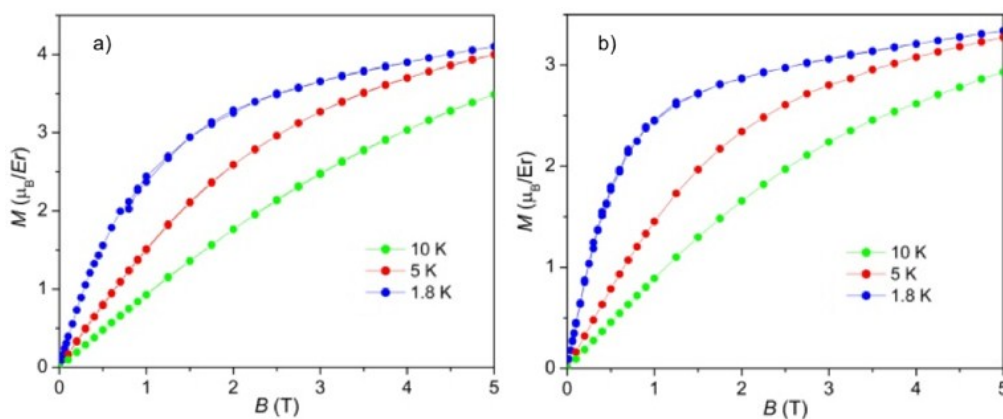
Figure S11. Field dependence of the magnetization at several temperatures for (a) LErH (**3**) and (b) LYH:0.065Er (**3'**).
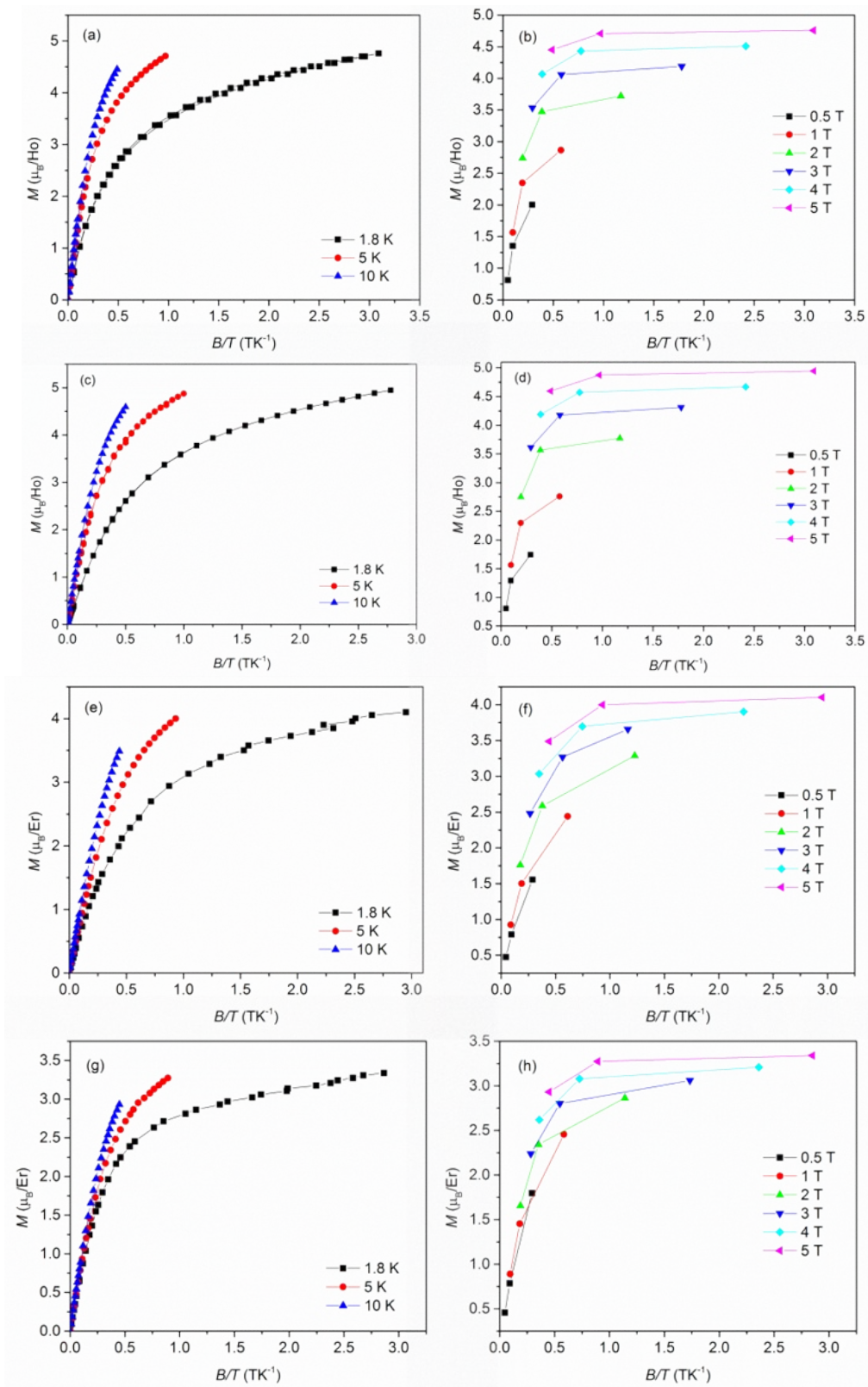
Figure S12. Reduced magnetization plots a) and b) LHoH (**2**); c) and d) LYH:0.045Ho (**2'**); e) and f) LErH (**3**); g) and h) LYH:0.069Er (**3'**).

b) AC measurements

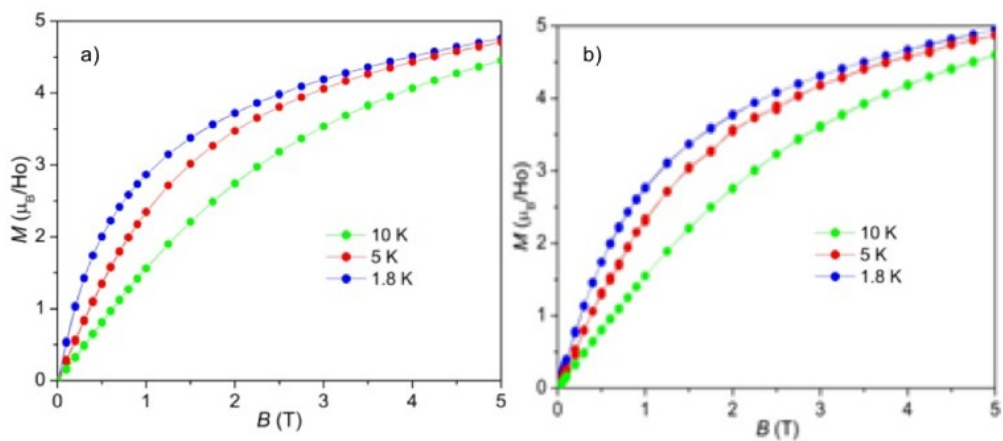**Figure S13.** Temperature dependence of the (a) real, χ', and (b) imaginary, χ'', components of the AC susceptibility for LTbH (**1**), at different frequencies under a static field of H_{DC} = 0 Oe. H_{AC} = 5 Oe.

Figure S14. Temperature dependence of the (a) real, χ', and (b) imaginary, χ'', components of the AC susceptibility for LTbH (**1**), at different frequencies under a static field of H_{DC} = 1000 Oe. H_{AC} = 5 Oe.

Figure S15. Temperature dependence of the (left) real, χ′, and (right) imaginary, χ″, components of the AC susceptibility for LHoH (**2**) a) and b), and LErH (**3**) c) and d), at different frequencies under a static field of H_{DC} = 1000 Oe. H_{AC} = 5 Oe.

Figure S16. Temperature dependence of the (a) real, χ′, and (b) imaginary, χ″, components of the AC susceptibility for LYH:0.044Tb (**1'**), collected at different AC frequencies under a static field of H_{DC} = 0 Oe. H_{AC} = 5 Oe.

Figure S17. Temperature dependence of the (a) real, χ', and (b) imaginary, χ'', components of the AC susceptibility for LYH:0.045Ho (**2'**), collected at different AC frequencies under a static field of H_{DC} = 0 Oe. H_{AC} = 5 Oe.

Figure S18. Temperature dependence of the (a) real, χ', and (b) imaginary, χ'', components of the AC susceptibility for LYH:0.065Er (**3'**), collected at different AC frequencies under a static field of H_{DC} = 0 Oe. H_{AC} = 5 Oe.
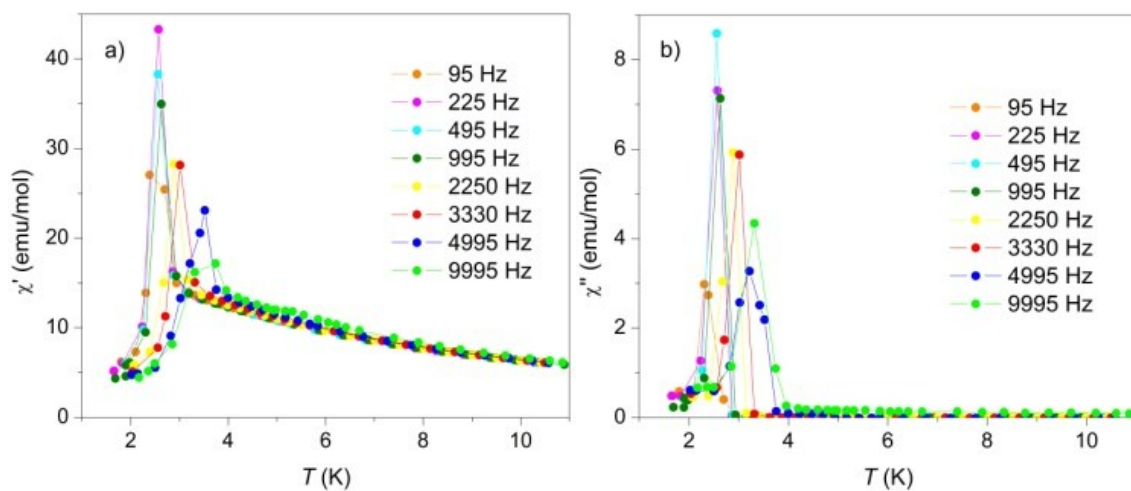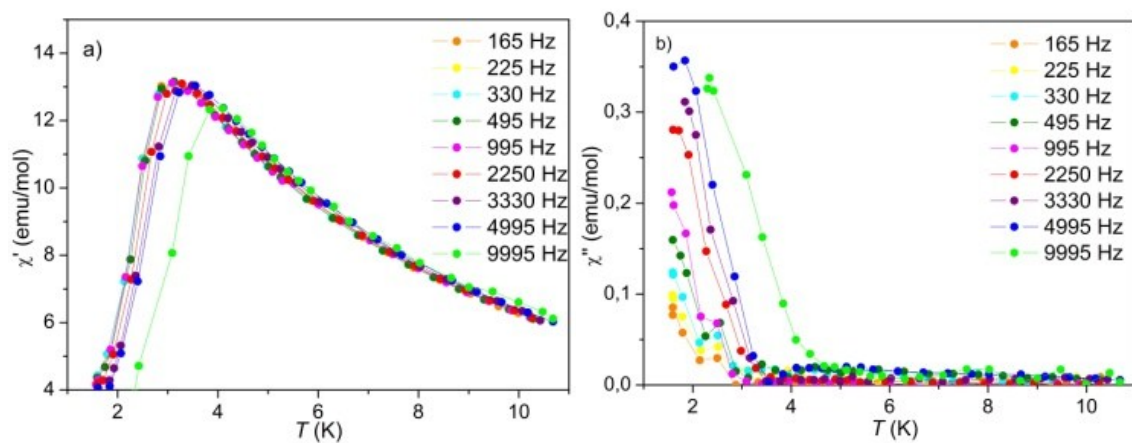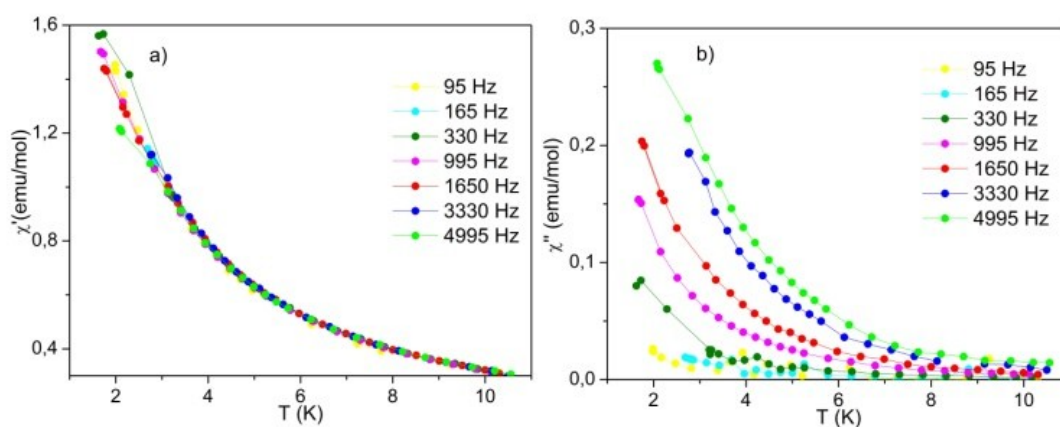

Figure S19. Temperature dependence of the (a) real, χ', and (b) imaginary, χ'', components of the AC susceptibility for LYH:0.044Tb (**1'**), at different frequencies under a static field of H_{DC} = 1000 Oe. H_{AC} = 5 Oe.
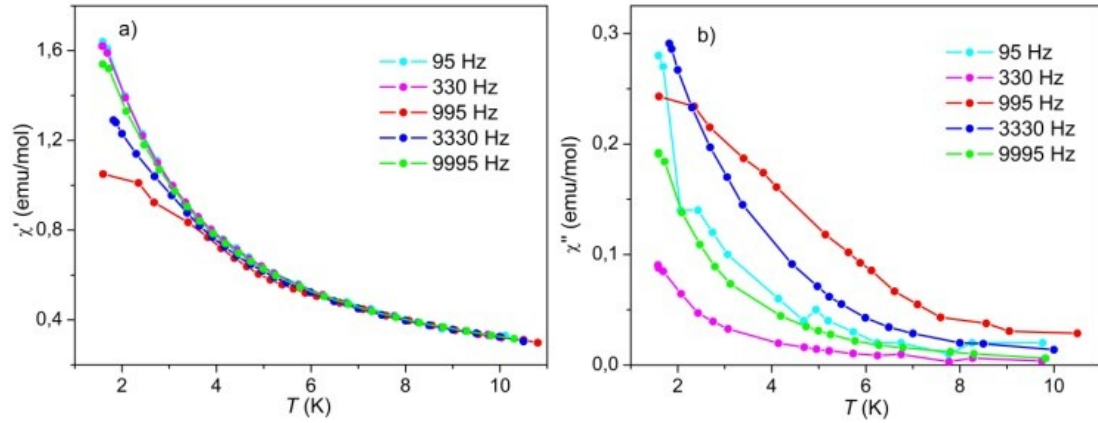
Figure S20. Temperature dependence of (a) real, χ′, and (b) imaginary, χ′′, components of the AC susceptibility for LYH:0.045Ho (**2′**), at different frequencies under a static field of H_{DC} = 1000 Oe. H_{AC} = 5 Oe.
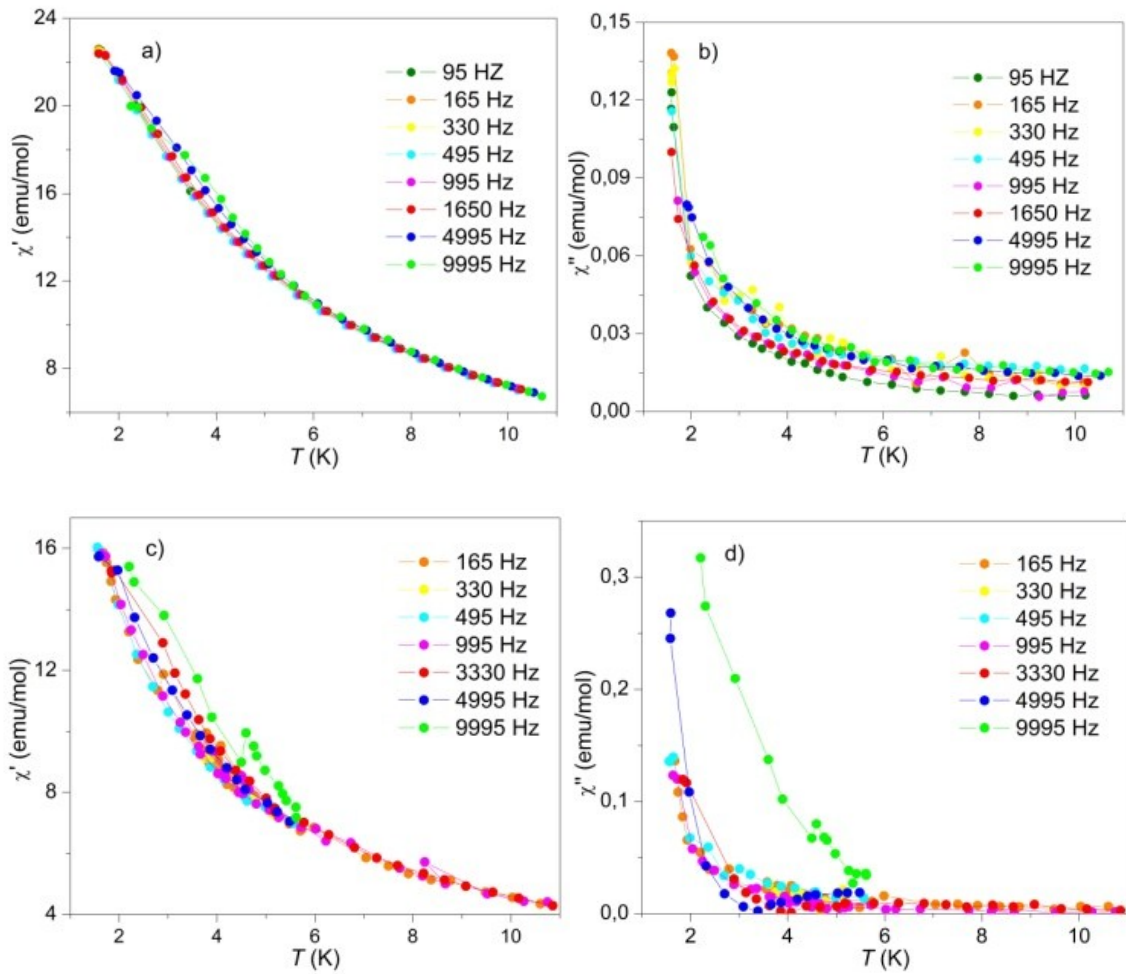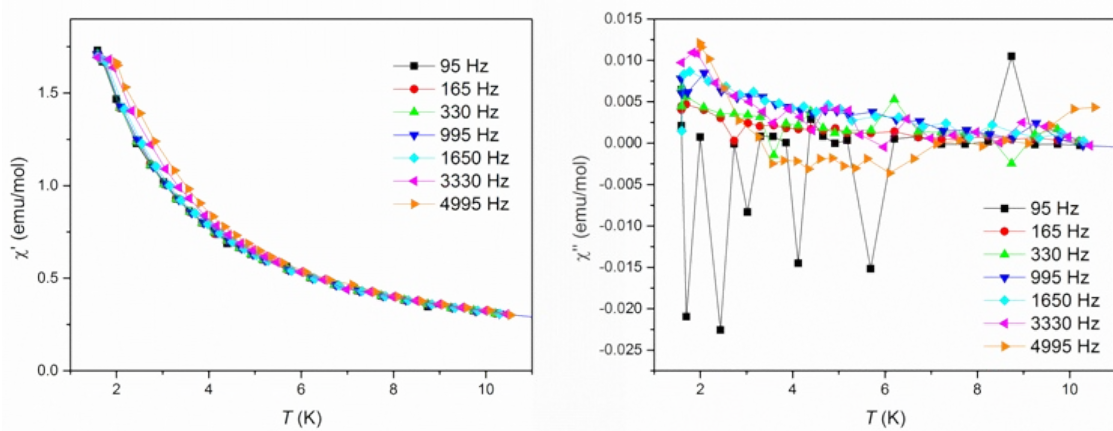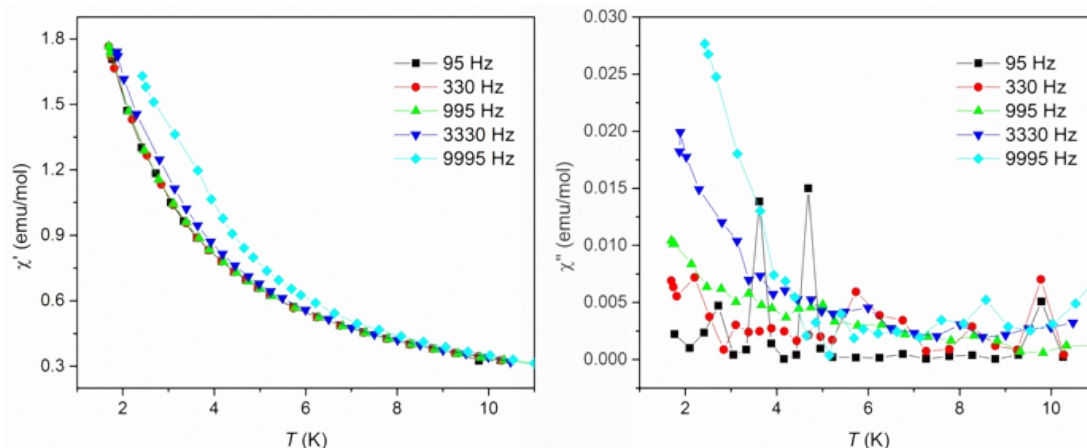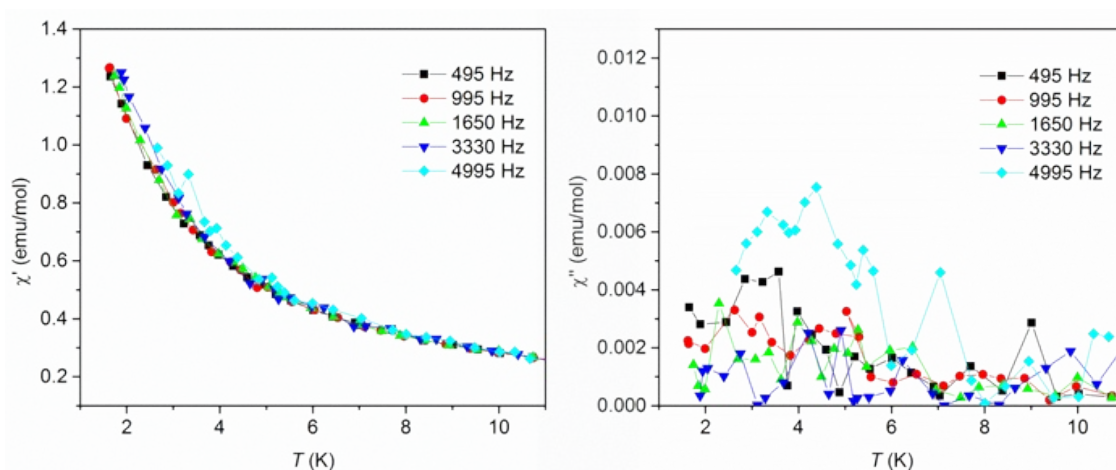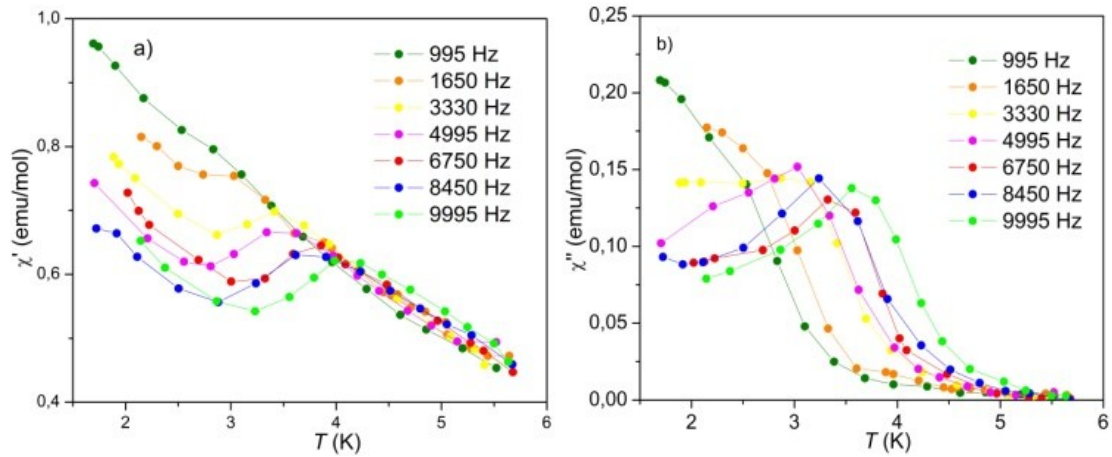

Figure S21. Temperature dependence of the (a) real, χ′, and (b) imaginary, χ′′, components of the AC susceptibility for LYH:0.065Er (**3′**), at different frequencies under a static field of H_{DC} = 1000 Oe. H_{AC} = 5 Oe.

Table S1. Generalized Debye model fitting parameters under a static field of H_{DC} = 1000 Oe, in the temperature range of 1.6 to 6.0 K, for LYH:0.044Tb (**1′**).

T (K)	α	τ (s)	χ_S (emu.mol^{-1})	χ_T (emu.mol^{-1})
1.6	0.21333	3.63777E-5	1.65	1.71366
2.2	0.138	3.29087E-5	0.83531	1.40163
2.5	0.1156	3.06609E-5	0.77876	1.26701
3.1	0.11141	2.65088E-5	0.67026	1.0738
3.4	0.12469	2.41532E-5	0.61631	1.00204
3.9	0.13035	2.18261E-5	0.54276	0.85766
4.4	0.15222	1.95828E-5	0.48754	0.7531
5.0	0.15822	1.70745E-5	0.44118	0.66984
5.5	0.16715	1.51465E-5	0.4092	0.60395
6.0	0.2009	1.3799E-5	0.38901	0.55223

Table S2. Generalized Debye model fitting parameters under a static field of H_{DC} = 1000 Oe, in the temperature range of 1.8 to 5.0 K, for LYH:0.045Ho (**2'**).

$T\ (K)$	α	τ (s)	χ_S $(emu.mol^{-1})$	χ_T $(emu.mol^{-1})$
1.8	0.13393	4.47E-05	0.9088	1.6401
2.2	0.1403	3.93E-05	0.80842	1.44432
2.4	0.15002	3.40E-05	0.72804	1.29549
2.6	0.16296	3.06E-05	0.66819	1.1857
2.8	0.13681	3.17E-05	0.6525	1.09014
3.0	0.13992	2.95E-05	0.61252	1.01527
3.5	0.15983	2.54E-05	0.53136	0.86816
4.0	0.15531	2.41E-05	0.48675	0.75781
4.5	0.19744	1.68E-05	0.41272	0.67117
5.0	0.19879	1.59E-05	0.39926	0.60489

Table S3. Generalized Debye model fitting parameters under a static field of H_{DC} = 1000 Oe, in the temperature range of 1.6 to 3.6 K, for LYH:0.065Er (**3'**).

$T\ (K)$	α	τ (s)	χ_S $(emu.mol^{-1})$	χ_T $(emu.mol^{-1})$
1.6 K	0.16254	1.53585E-4	0.66296	1.25428
2.6 K	0.0923	7.06064E-5	0.51748	0.9076
2.8 K	0.10286	4.23429E-5	0.48831	0.842
3.1 K	0.09938	2.669E-5	0.48026	0.78976
3.6 K	0.16711	1.57604E-5	0.53812	0.68081

Assuming that the relaxation of the magnetization process simply occurs through an Orbach mechanism, a fit of the Arrhenius law (Eq. S1) based on an exponential temperature dependence was performed:

$$\tau(T) = \tau_0 \exp(\Delta/k_B T) \qquad \text{(Eq. S1)},$$

where τ_0, Δ, and k_B are the pre-exponential factor, the relaxation energy barrier, and the Boltzmann constant, respectively. As shown in Figure S22, the fit deviates from linearity at low temperatures being only valid at temperatures higher than 3.9 K, 2.6 K and 2.6 K, with the following parameters: U_{eff} = 5.39 K with τ_0 = 5.7x10^{-6} s, U_{eff} = 2.23 K with τ_0 = 1.44x10^{-5} s, and U_{eff} = 14.1 K with τ_0 = 3.07x10^{-7} s, for **1'**, **2'**, and **3'**, respectively.
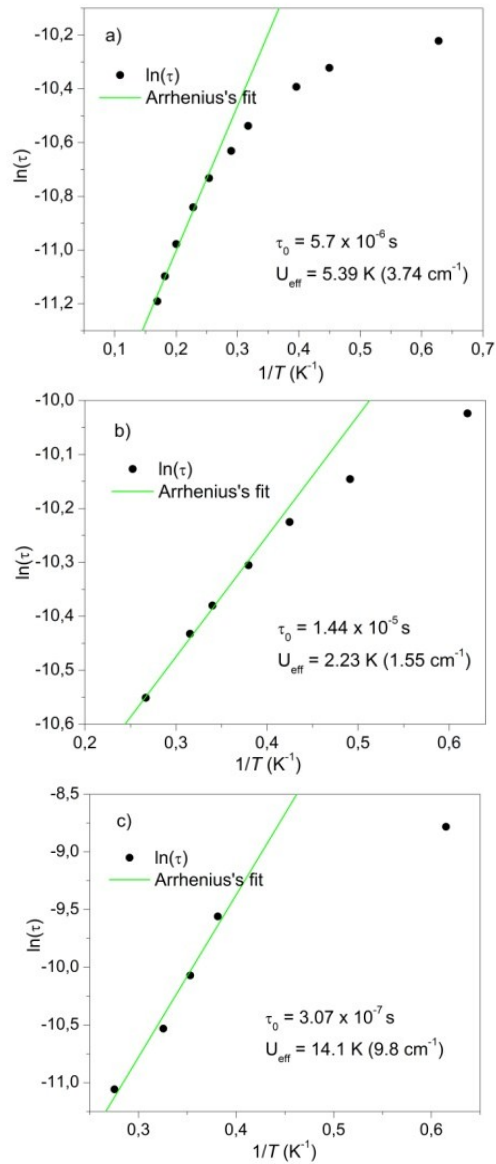

Figure S22. Thermal dependence of the relaxation time τ, measured using an AC field of H_{AC} = 5 Oe and under a static field of H_{DC} = 1000 Oe for (a) **1'** (LYH:0.044Tb), (b) **2'** (LYH:0.045Ho), and (c) **3'** (LYH:0.065Er). The lines are fits to the Arrhenius equation (eq. 2), assuming an Orbach process.

3) Radial effective charge (REC) model

The REC model is an electrostatic *semi-empirical* crystal field approach commonly used in molecular magnetism, which allows to provide an estimation of the crystal field parameters (CFPs) and then modelling the static magnetic properties.[2] Through this procedure, the model also gives an estimation of the ground multiplet energy levels and their corresponding wave functions. This kind of calculations start with the crystallographic/non-idealized atomic coordinates of the first coordination sphere around the *f*-block element. These are introduced as an input in the software code SIMPRE,[3] which parameterizes the electric field effect produced by the surrounding ligands by using the following Crystal Field Hamiltonian expressed in terms of the Extended Stevens Operators (ESOs)[4]:

$$\hat{H}_{cf}(J) = \sum_{k=2,4,6} \sum_{q=-k}^{k} B_k^q O_k^q = \sum_{k=2,4,6} \sum_{q=-k}^{k} a_k (1-\sigma_k) A_k^q \left\langle r^k \right\rangle O_k^q$$

(Eq. S2)

where k is the order (also called rank or degree) and q is the operator range, that varies between k and $-k$, of the Stevens operator equivalents O_k^q as defined by Ryabov in terms of the angular momentum operators $J_\pm$ and J_z,[5] where the components $O_k^q(c)$ and $O_k^q(s)$ correspond to the ESOs with q ≥ 0 and q < 0 respectively.[8] Note that all the Stevens CF parameters B_k^q are real, whereas the matrix elements of O_k^q (q < O) are imaginary. a_k are the α, β and γ Stevens coefficients[6] for k = 2, 4, 6, respectively, which are tabulated and depend on the number of f electrons. σ_k are the Sternheimer shielding parameters[7] of the 4f electronic shell, and <r^k> are the expectation values of the radius.[10]

In the model, the A_k^q CF parameters are calculated through the following expressions:

$$A_k^0 = \frac{4\pi}{2k+1} \sum_{i=1}^{N} \frac{Z_i e^2}{R_i^{k+1}} Z_{k0}(\theta_i, \varphi_i) p_{kq}$$

(Eq. S3.a)

$$A_k^q = \frac{4\pi}{2k+1} \sum_{i=1}^{N} \frac{Z_i e^2}{R_i^{k+1}} Z_{kq}^c(\theta_i, \varphi_i) p_{kq}$$

(Eq. S3.b)

$$A_k^q = \frac{4\pi}{2k+1} \sum_{i=1}^{N} \frac{Z_i e^2}{R_i^{k+1}} Z_{k|q|}^s(\theta_i, \varphi_i) p_{k|q|}$$

(Eq. S3.c)

and the effect of the ligand is modeled through an effective point charge situated between the lanthanide and the coordinated atom at a distance R_i from the magnetic centre, which is smaller than the real metal-ligand distance (r_i). To account for the effect of covalent electron sharing, a radial displacement vector (D_r) is defined, in which the polar coordinate r of each coordinated atom is varied, $R_i = r_i - D_r$. The usual procedure is to obtain the D_r parameter of each kind of donor atom from a collective fit of an observable (e.g. energy levels or magnetic properties) for a family of isostructural lanthanide complexes. At the same time, the charge value (Z_i) is scanned in order to achieve the minimum deviation between calculated and

experimental data, whereas θ_i and φ_i remain constant. Thus, we have performed a collective fit using the first coordination sphere of the different magnetic centres for each of the systems of the LLH family, with the exception of Ho3 and Er3, which presented some of the H_2O molecules much closer (Ho3-O ($H2O$) bond distance is 2.3634(7) Å, while Er3-O bond distance is 2.3742(9) Å) to the central ion and could artificially govern the results of the fit. The resulting collective D_r and Z_i were 1.17 Å and 0.04, respectively. Subsequently, both parameters were slightly varied in order to provide a more suitable phenomenological description of each compound. The resulting set of REC parameters is reported in Table S5.

Table S4. REC parameters obtained for each lanthanide.

	D_r (Å)	Z_i
Tb	1.33	0.03
Dy	1.17	0.04333
Ho	1.31	0.02
Er	1.17	0.01333

The application of these parameters to the first coordination sphere of the lanthanide allowed us to estimate the crystal field parameters (CFPs), energy levels, wave functions and magnetic properties. The reported differences in the coordination environment yield different ground-state m_J compositions for the different crystallographic sites. The calculated energy levels and m_J compositions are reported as follows in Tables S5-S8.

Table S5. Ground multiplet energy levels calculated by the REC model for each Tb center. % M_J contributions are only considered for values greater than 10%.

Energy levels of Tb1 (cm^{-1})	Amplitude of $\|M_J\rangle$	Energy levels of Tb2 (cm^{-1})	Amplitude of $\|M_J\rangle$	Energy levels of Tb3 (cm^{-1})	Amplitude of $\|M_J\rangle$
0	15% |±2> + 59% |0>	0	20% |±2> + 50% |0>	0	50% |±6>
3.3	41% |±1>	2.0	40% |±1>	0.02	50% |±6>
41.0	18% |±6> + 11% |±4> + 10% |±2>	128.2	18% |±2> + 10% |±1>	120.0	46% |±5>
71.8	18% |±6> + 10% |±4>	143.4	25% |±3> + 20% |±5>	122.4	47% |±5>
131.1	10% |±5> + 19% |±3>	162.7	10% |±5> + 18% |±4> + 13% |±1> + 12% |0>	213.4	13% |±4> + 11% |±2> + 13% |±1>
186.7	10% |±5> + 20% |±3>	168.7	24% |±3>	221.2	13% |±4> + 17% |±3> + 13% |±2>
276.6	17% |±1>	218.2	23% |±4> + 17% |0>	271.5	12% |±3> + 20% |±1> + 22% |0>
350.7	13% |±5> + 16% |±3> + 12% |±2>	222.3	10% |±6> + 29% |±5>	277.2	10% |±4> + 17% |±2> + 33% |0>
390.7	25% |±6> + 14% |±4>	224.8	10% |±6> + 28% |±5> + 10% |±4>	296.3	22% |±4> + 17% |±1>
411.1	19% |±6> + 15% |±2>	291.1	20% |±6>	341.6	17% |±4> + 32% |0>
514.3	14% |±5> + 13% |±3> + 10% |0>	316.4	17% |±6>	393.6	10% |±4> + 14% |±3> + 21% |±1>
573.6	11% |±4> + 11% |±2> + 20% |0>	364.8	20% |±6> + 10% |±4>	523.2	21% |±3> + 14% |±2>
631.4	17% |±4> + 16% |±1>	375.1	20% |±6> + 12% |±3>	531.6	18% |±3> + 24% |±2>

Table S6. Ground multiplet Kramers doublets calculated by the REC model for each Dy center. % M_J contributions are only considered for values greater than 10%.

Energy levels of Dy1 (cm⁻¹)	Amplitude of |M_J>	Energy levels of Dy2 (cm⁻¹)	Amplitude of |M_J>	Energy levels of Dy3 (cm⁻¹)	Amplitude of |M_J>
0	64% |±11/2>	0	89% |±15/2>	0	92% |±15/2>
25.8	11% |±13/2> + 25% |±9/2> + 12% |±1/2>	30.8	67% |±9/2> + 16% |±7/2>	57.0	25% |±9/2> + 30% |±7/2> + 25% |±5/2>
64.3	41% |±13/2> + 19% |±9/2>	75.4	48% |±11/2> + 40% |±7/2>	93.8	32% |±13/2> + 47% |±11/2> + 13% |±9/2>
100.4	19% |±13/2> + 10% |±11/2> + 21% |±9/2> + 17% |∓7/2>	114.9	29% |±13/2> + 13% |±9/2> + 15% |±7/2> + 22% |±5/2>	127.6	39% |±9/2> + 10% |∓7/2>
146.9	10% |±11/2> + 17% |±7/2> + 11% |±5/2> + 10% |±3/2> + 18% |∓7/2>	177.5	33% |±13/2> + 32% |±11/2>	154.6	41% |±13/2> + 35% |±11/2>
222.0	20% |±5/2> + 13% |±1/2> + 16% |∓3/2> + 15% |∓5/2>	213.6	23% |±13/2> + 49% |±5/2>	215.6	34% |±7/2> + 18% |±5/2> + 15% |±3/2>
288.1	78% |±15/2>	287.1	54% |±3/2> + 26% |∓1/2>	280.0	38% |±5/2> + 28 |±3/2> + 15% |±1/2>
335.4	10% |±5/2> + 19% |±3/2> + 20% |±1/2> + 19% |∓1/2> + 10% |∓3/2>	492.9	58% |±1/2> + 26% |∓3/2>	328.9	32% |±3/2> + 41% |±1/2> + 19% |∓1/2>

Table S7. Ground multiplet energy levels calculated by the REC model for each Ho center. % M_J contributions are only considered for values greater than 10%.

Energy levels of Ho1 (cm⁻¹)	Amplitude of |M_J>	Energy levels of Ho2 (cm⁻¹)	Amplitude of |M_J>	Energy levels of Ho3 (cm⁻¹)	Amplitude of |M_J>
0	49% |0>	0	11% |±6> + 10% |±3> + 44% |0>	0	11% |±2> + 49% |0>
2.0	31% |±1>	8.1	12% |±7> + 10% |±4> + 23% |±1>	0.7	34% |±1>
53.2	15% |±7> + 11% |±6> + 11% |±2>	17.3	22% |±7> + 10% |±1>	136.5	15% |±7> + 10% |±2>
73.3	20% |±7> + 15% |±1>	75.9	17% |±5>	155.5	17% |±7> + 12% |±6> + 11% |±1>
90.1	16% |±7> + 13% |±2> + 10% |±1>	102.1	22% |±7> + 20% |±2>	212.9	26% |±8> + 12% |0>
167.1	11% |±8> + 12% |±3>	113.7	10% |±8> + 15% |±5>	322.9	13% |±8> + 14% |±3>
213.4	11% |±8> + 11% |±5>	122.3	36% |±6>	368.7	14% |±8> + 14% |±3>
234.6	12% |±4> + 16% |±3>	157.8	11% |±7> + 15% |±3>	455.2	18% |±6> + 14% |±3>
244.9	17% |±8> + 13% |±6>	182.9	15% |±3> + 11% |±1> + 12% |0>	457.2	12% |±7> + 19% |±2>
342.8	18% |±6>	198.8	10% |±2> + 17% |±1> + 14% |0>	565.6	11% |±5> + 17% |±3> + 11% |±2>
377.4	27% |±6> + 10% |±1>	255.8	15% |±8> + 12% |±1>	579.2	28% |±4>
399.1	12% |±8> + 13% |±7>	257.7	15% |±6> + 29% |0>	583.8	14% |±5> + 17% |±2>
453.7	11% |±5> + 19% |±4>	283.5	27% |±4>	624.1	12% |±6>
487.6	12% |±8> + 20% |±5> + 14% |±2>	286.8	13% |±8> + 12% |±5> + 20% |±3>	679.7	15% |±8> + 11% |±3>
522.2	12% |±8> + 21% |±3>	328.7	20% |±8> + 16% |±5>	697.4	21% |±8> + 11% |±3>
572.8	12% |±5> + 14% |±3> + 16% |0>	369.6	10% |±5> + 25% |±3>	741.9	12% |±5> + 13% |±4>
577.1	22% |±4> + 12% |±1>	370.5	25% |±4> + 16% |±2>	749.4	18% |±5> + 11% |±4> + 19% |0>

Table S8. Ground multiplet Kramers doublets calculated by the REC model for each Er center. % M_J contributions are only considered for values greater than 10%.

Energy levels of Er1 (cm^{-1})	Amplitude of $\|M_J\rangle$	Energy levels of Er2 (cm^{-1})	Amplitude of $\|M_J\rangle$	Energy levels of Er3 (cm^{-1})	Amplitude of $\|M_J\rangle$
0	99% |±13/2>	0	70% |±7/2> + 25% |∓5/2>	0	100% |±13/2>
131.7	19% |±11/2> + 35% |±1/2> + 43% |∓1/2>	33.7	26% |±15/2> + 63% |±9/2>	366.3	96% |±1/2>
179.5	78% |±11/2> + 15% |∓1/2>	89.5	66% |±5/2> + 20% |∓7/2>	491.2	98% |±11/2>
258.7	93% |±3/2>	108.7	59% |±15/2> + 12% |±9/2> + 15% |∓3/2>	762.0	96% |±3/2>
420.1	54% |±9/2> + 38% |±5/2>	161.3	11% |±11/2> + 11% |±9/2> + 18 |±3/2> + 19% |∓1/2> + 20% |∓3/2>	1175.6	45% |±9/2> + 55% |±5/2>
439.8	41% |±9/2> + 51% |±5/2>	174.2	53% |±11/2> + 16% |±3/2> + 14% |∓1/2>	1360.8	55% |±9/2> + 44% |±5/2>
521.3	83% |±7/2>	234.0	35% |±11/2> + 44% |∓1/2>	1541.2	97% |±7/2>
589.5	89% |±15/2>	303.6	90% |±13/2>	1721.1	96% |±15/2>

References

1. F. Geng, Y. Matsushita, R. Ma, H. Xin, M. Tanaka, F. Izumi, N. Iyi, T. Sasaki, *J. Am. Chem. Soc.*, 2008, **130**, 16344.

2. Baldoví, J. J.; Borrás-Almenar, J. J.; Clemente-Juan, J. M.; Coronado, E.; Gaita-Ariño, A. *Dalton Trans.* **2012**, *41*, 13705

3. Baldoví, J. J.; Cardona-Serra, S.; Clemente-Juan, J. M.; Coronado, E.; Gaita-Ariño, A.; Palii, A. *J. Comput. Chem.* **2013**, *34*, 1961–1967

4. C. Rudowicz, C.Y. Chung, *J. Phys. Condens. Matter*, 2004, **16**, 5825; (b) C. Rudowicz, 1985, *J. Phys. C: Solid State Phys.*, **18**, 1415; (c) C. Rudowicz, 1985b, *J. Phys. C: Solid State Phys.*, **18**, 3837 (erratum)

5. I.D. Ryabov, *Journal of Magnetic Resonance*, 1999*, **140**, 141

6. K. W. H. Stevens, *Proc.Phys. Soc.* **1952**, *65*, 209

7. S. Edvardsson, M. Klinterberg, *Journal of Alloys and Compounds,* **1998**, 275, 233